1	Ancestral admixture is the main determinant of global biodiversity in
2	fission yeast
3	
4	
5	
6 7	Sergio Tusso <sup>1,2,*</sup> , Bart P.S. Nieuwenhuis <sup>1</sup> , Fritz J. Sedlazeck <sup>3</sup> , John W. Davey <sup>4</sup> , Daniel C. Jeffares <sup>5,6</sup> , Jochen B. W. Wolf <sup>1,2,*</sup>
8 9 10 11	<sup>1</sup> Division of Evolutionary Biology, Faculty of Biology, LMU Munich, Grosshaderner Str. 2, 82152 Planegg- Martinsried, Germany
12 13 14	<sup>2</sup> Science for Life Laboratories and Department of Evolutionary Biology, Norbyvägen 18D, 75236 Uppsala University, 75236 Uppsala, Sweden
15 16	<sup>3</sup> Human Genome Sequencing Center, Baylor College of Medicine, One Baylor Plaza, Houston TX 77030
17 18 19	<sup>4</sup> Bioscience Technology Facility, Department of Biology, University of York, Wentworth Way, York YO10 5DD, United Kingdom
20 21	<sup>5</sup> Department of Biology, University of York, Wentworth Way, York YO10 5DD, United Kingdom
22	<sup>6</sup> York Biomedical Research Institute (YBRI), University of York, Wentworth Way, York YO10 5DD, United
23	Kingdom
24 25 26	
27 28 29	* Authors to whom correspondence should be addressed
30 31	Corresponding authors:
32	Sergio Tusso: situssog@gmail.com
33 34	Jochen B. W. Wolf: j.wolf@biologie.uni-muenchen.de
35	

36 Mutation and recombination are key evolutionary processes governing phenotypic 37 variation and reproductive isolation. We here demonstrate that biodiversity within all globally known strains of Schizosaccharomyces pombe arose through admixture between 38 two divergent ancestral lineages. Initial hybridization occurred ~20 sexual outcrossing 39 generations ago consistent with recent, human-induced migration at the onset of 40 intensified transcontinental trade. Species-wide heritable phenotypic variation was 41 explained near-exclusively by strain-specific arrangements of alternating ancestry 42 components with evidence for transgressive segregation. Reproductive compatibility 43 between strains was likewise predicted by the degree of shared ancestry. To assess the 44 45 genetic determinants of ancestry block distribution across the genome, we characterized the type, frequency and position of structural genomic variation (SV) using nanopore 46 and single-molecule real time sequencing, discovering over 800 SVs. Despite being 47 48 associated with double-strand break initiation points, SV exerted overall little influence 49 on the introgression landscape or on reproductive compatibility that exist between 50 strains. In contrast, we find strongly increased statistical linkage between ancestral 51 populations that is consistent with negative epistatic selection shaping genomic ancestry combinations during the course of hybridization. This study provides a detailed, 52 experimentally tractable example that genomes of natural populations are mosaics 53 54 reflecting different evolutionary histories. Exploiting genome-wide heterogeneity in the history of ancestral recombination and lineage-specific mutations sheds new light on the 55 population history of S. pombe and highlights the importance of hybridization as a 56 creative force in generating biodiversity. 57

58

59

# 61 Introduction

62	Mutation is the ultimate source of biodiversity. In sexually reproducing organisms it is
63	assisted by recombination shuffling mutations of independent genomic backgrounds into
64	millions of novel combinations. This widens the phenotypic space upon which selection can
65	act and thereby accelerates evolutionary change (Muller, 1932; Fisher, 1999; McDonald et al.,
66	2016). This effect is enhanced for heterospecific recombination between genomes of
67	divergent populations (Abbott et al., 2013). Novel combinations of independently
68	accumulated mutations can significantly increase the overall genetic and phenotypic variation,
69	even beyond the phenotypic space of parental lineages (transgressive segregation
70	(Lamichhaney et al., 2017; Nolte and Sheets, 2005)). Yet, if mutations of the parental
71	genomes are not compatible to produce viable and fertile offspring, hybridization is a dead
72	end. Phenotypic variation then remains within the confines of genetic variation of each
73	reproductively isolated, parental lineage.
74	

74

75 It is increasingly recognised that hybridization is commonplace in nature, and constitutes an 76 important driver of diversification (Abbott et al., 2013; Mallet, 2005). Ancestry components 77 of hybrid genomes can range from clear dominance of alleles from the more abundant species 78 (Dowling et al., 1989; Taylor and Hebert, 1993), over a range of admixture proportions 79 (Lamichhaney et al., 2017; Runemark et al., 2018) to the transfer of single adaptive loci (The 80 Heliconius Genome Consortium et al., 2012). The final genomic composition is determined 81 by a complex interplay of demographic processes, heterogeneity in recombination (e.g. 82 induced by genomic rearrangements) (Wellenreuther and Bernatchez, 2018) and selection 83 (Sankararaman et al., 2014; Schumer et al., 2016). Progress in sequencing technology, now 84 allows characterisation of patterns of admixture and the illumination of underlying processes 85 (Payseur and Rieseberg, 2016). Yet, research has largely focused on animals (Turner and Harr,

86	2014; Vijay et al., 2016; Meier et al., 2017; Jay et al., 2018) and plants (Twyford et al., 2015)
87	characterized by large genomes and long generation times. Relatively little attention has been
88	paid to natural populations of sexually reproducing micro-organisms (Leducq et al., 2016;
89	Stukenbrock, 2016; Peter et al., 2018; Steenkamp et al., 2018).
90	
91	The fission yeast Schizosaccharomyes pombe is an archiascomycete haploid unicellular
92	fungus with a facultative sexual mode of reproduction. Despite of its outstanding importance
93	as a model system in cellular biology (Hoffman et al., 2015) and the existence of global
94	sample collections, essentially all research has been limited to a single isogenic strain isolated
95	by Leupold in 1949 (Leupold 972; JB22 in this study). Very little is known about the ecology,
96	origin, and evolutionary history of the species (Jeffares, 2018). Global population structure
97	has been described shallow with no apparent geographic stratification (Jeffares et al., 2015).
98	Genetic diversity ( $\pi = 3 \times 10^{-3}$ substitutions/site) appears to be strongly influenced by genome-
99	wide purifying selection with the possible exception of region-specific balancing selection
100	(Fawcett et al., 2014; Jeffares et al., 2015). Despite the overall low genetic diversity, S. pombe
101	shows abundant additive genetic variation in a variety of phenotypic traits including growth,
102	stress responses, cell morphology, and cellular biochemistry (Jeffares et al., 2015). The
103	apparent worldwide lack of genetic structure in this species appears inconsistent with the large
104	phenotypic variation between strains and with evidence for post-zygotic reproductive
105	isolation between inter-strain crosses, ranging from 1% to 90 % of spore viability
106	(Kondrat'eva and Naumov, 2001; Teresa Avelar et al., 2013; Zanders et al., 2014; Jeffares et
107	al., 2015; Naumov et al., 2015; Marsellach, 2017).
108	
109	In this study, we integrate whole-genome sequencing data from three different technologies -

sequencing-by-synthesis (Illumina technology data accessed from (Jeffares et al., 2015)),

111 single-molecule real-time sequencing (Pacific BioSciences technology, this study) and 112 nanopore sequencing (Oxford Nanopore technology, this study) - sourced from a mostly 113 human-associated, global sample collection to elucidate the evolutionary history of the S. 114 *pombe* complex. Using population genetic analyses based on single nucleotide polymorphism 115 (SNP) we show that global genetic variation and heritable phenotype variation of S. pombe 116 results from recent hybridization of two ancient lineages. 25 de novo assemblies from 17 117 divergent strains further allowed us to quantify segregating structural variation including 118 insertions, deletions, inversion and translocations. In light of these findings, we retrace the 119 global population history of the species, and discuss the relative importance of genome-wide 120 ancestry and structural mutations in explaining phenotypic variation and reproductive 121 isolation.

122

- 123 **Results**
- 124

#### 125 Global genetic variation in *S. pombe* is characterized by ancient admixture

126 Genetic variation of the global S. pombe collection comprises 172,935 SNPs segregating in 127 161 strains. Considering SNPs independently, individuals can be sub-structured into 57 clades 128 that differ by more than 1900 variants, but are near-clonal within clades (Jeffares et al., 2015). 129 To examine population ancestry further, we divided the genome into 1925 overlapping 130 windows containing 200 SNP each and one representative from each clade (57 samples in 131 total). Principle component analysis conducted on each orthologous window showed a highly 132 consistent pattern along the genome (Figure 1a, Supplementary Figure 1): i) the major axis 133 of variation (PC1) split all samples into two clear discrete groups explaining  $60\% \pm 13\%$  of 134 genetic variance (Figure 1b). ii) All samples fell into either extreme of the normalized distribution of PC1 scores (*PC*1  $\in$  [0; 0.3]  $\cup$  [0.7; 1]) (Supplementary Figures 2 & 3) 135

136 with the only exception of strains with inferred changes in ploidy level (Methods,

137 **Supplementary Figure 4**). iii) PC2 explained  $13\% \pm 6\%$  of variation and consistently 138 attributed higher variation to one of the two groups. This strong signal of genomic windows 139 separating into two discrete groups suggested that the genomic diversity in this collection was 140 derived from two distinct populations. However, iv) group membership of strains changes 141 among windows moving along the genome, reflecting recombination between these two well 142 defined groups. This last point highlights the importance of considering haplotype structure 143 and explains the lack of observed population structure when disregarding non-independence 144 of SNPs (Jeffares et al., 2015).

145

146 The strong signal from the PCA that systematically differentiates between groups along the 147 genome were likewise reflected in population genetic summary statistics including 148 Watterson's theta ( $\theta$ ), pairwise nucleotide diversity ( $\pi$ ), and Tajima's D (**Figure 1d and 2**). Significant differences in these statistics (Kendall's  $\tau$  p-value  $\leq 2.2 \times 10^{-16}$ ), were also present 149 150 in mitochondrial genetic variation (Figure 1a), allowed polarising the two groups across 151 windows into a 'low-diversity' group (red) and a 'high-diversity group (blue) (Figure 1a, 152 **Supplementary Figure 5**). Genetic divergence between groups (D<sub>xv</sub>) was 15 and 3 times 153 higher than mean genetic diversity ( $\pi$ ) within each group, respectively, and thus supports a 154 period of independent evolution. Painting genomic windows by group membership revealed 155 blocks of ancestry distributed in sample specific patterns along the genome (Figure 1c, 156 Supplementary Figure 6). The sample corresponding to the reference genome isolated 157 originally from Europe (Leupold's 972; JB22) consisted almost exclusively of 'red' ancestry 158 (>96% red), whereas other samples were characterized near-exclusively by 'blue' ancestry 159 (>96% blue). The sample considered to be a different species from Asia, S. kambucha 160 (JB1180 (Singh and Klar, 2002)) had a large proportion of 'blue' windows (>70% blue).

Hereafter, we refer to the 'red' and 'blue' clade as *Sp* and *Sk*, for *S. pombe* and *S. kambucha*respectively. Grouping samples by the pattern of genomic ancestry across the genome
revealed 8 discrete clusters (Figure 1c). Consistent with independent and/or recent
segregation of ancestral groups, cluster membership for several samples differed between
chromosomes (Figure 1c) and genome components (Supplementary Figures 7 & 8). This is
also reflected by low support in the relationship between the 8 discrete clusters.

167

168 The distribution of ancestry components was highly heterogeneous across the chromosome 169 (Figure 2a, Supplementary Figure 6). Most strains showed an excess of Sp ancestry in parts 170 of chromosome I, whereas several regions of chromosome III had an excess of Sk ancestry. 171 Failing to incorporate this genome-wide variation of admixture proportions can mimic 172 signatures of selection. For example, equal ancestry contributions for a certain genomic 173 region will yield high positive values of both Tajima's D (**Supplementary Figure 9**) and  $\pi$ 174 and may be mistaken as evidence for balancing selection. Strong skew in ancestry proportions 175 reduces both statistics to values of the prevailing ancestry and may appear as evidence for 176 selective sweeps (Figure 2b). Taking ancestry into account, however, there was no clear 177 signature of selection in either Sp or Sk genetic variation that could account for heterogeneity 178 in the genetic composition of hybrids (Supplementary Figure 9). Signatures of selection 179 identified previously (cf. Fawcett et al., 2014) are likely artefacts due to skewed ancestry 180 proportions rather than events of positive or balancing selection in the ancestral populations. 181 182 Overall, our results provide strong evidence for the presence of at least two divergent

182 Overall, our results provide strong evidence for the presence of at least two divergent 183 ancestral populations: one genetically diverse group (*Sk* clade) and a less diverse group (*Sp* 184 clade). We found a large range of ancestral admixture proportions between these two clades 185 broadly clustering samples into 8 weakly supported groups. These resemble clusters of strains previously identified by *Structure* and *fineStructure* without explicit modelling of ancestral admixture (Jeffares et al., 2015). Neglecting ancestry, Jeffares et al. (2015) argued that the shallow population structure likely results from extensive gene flow between clusters. Yet, considering the genome-wide distribution of *Sk* and *Sp* ancestry, and lack of geographical structure, suggest that the 8 clusters are derived from one or a few centres of ancient admixture (hybridization) without the need of subsequent or recent gene flow between them.

192

# 193 Age of ancestral lineages and timing of hybridization

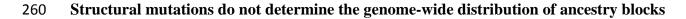
194 To shed further light on the population history, we estimated the age of the parental lineages 195 and the timing of initial hybridization. Calibrating mitochondrial divergence by known 196 collection dates over the last 100 years, Jeffares et al. (2015) estimated that the time to the 197 most recent common ancestor for all samples was around 2,300 years ago. Current 198 overrepresentation of near-pure Sp and Sk in Europe or Africa / Asia, respectively, is 199 consistent with an independent history of the parental lineages on different continents for the 200 most part of the last millennia (Supplementary Figure 8). Yet, the variety of admixed 201 genomes bears testimony to the fact that isolation has been disrupted by heterospecific gene 202 flow. Using a theoretical model assuming secondary contact with subsequent hybridization 203 (Janzen et al., 2018) we estimated that hybridization occurred within the last 20 sexual 204 outcrossing generations (Figure 3, Supplementary Figures 10 & 11). Considering 205 intermittent generations of asexual reproduction, high rates of haploid selfing and dormancy 206 of spores (Farlow et al., 2015; Jeffares, 2018) it is difficult to obtain a reliable estimate of 207 time in years. This recent estimate of hybridization is consistent with hybridization induced 208 by the onset of regular trans-continental human trade between Europe with Africa and Asia 209 (~14th century) and with the Americas (~16th century), with fission yeast as a human 210 commensal (Jeffares, 2018). This fits with the observation that all current samples from the

211	Americas were hybrids, while samples with the purest ancestry stem from Europe, Africa and
212	Asia. Moreover, negative genome-wide Tajima's D estimates for both ancestral clades (mean
213	$\pm$ SD for Sp: -0.8 $\pm$ 0.9 and Sk: -0.7 $\pm$ 0.6) signal a period of recent expansion.
214	
215	Heritable phenotypic variation and reproductive isolation are governed by ancestry
216	components
217	Hybridization can lead to rapid evolution due to selection acting on the genetic and
218	phenotypic variation emerging after admixture (Muller, 1932; Fisher, 1999; McDonald et al.,
219	2016). We assessed the consequences of hybridization on phenotypic variation making use of
220	a large data set including 228 quantitative traits collected from the strains under consideration
221	here (Jeffares et al., 2015). Contrary to genetic clustering of hybrid genomes (Figure 1c),
222	samples with similar ancestry proportions did not group in phenotypic space described by the
223	first two PC-dimensions capturing 31% of the total variance across traits (Figure 4a).
224	Moreover, phenotypic variation of hybrids exceeded variation of pure strains (>0.9 ancestry
225	for $Sp$ or $Sk$ ). This was supported by trait specific analyses. We divided samples into three
226	discrete groups: pure Sp, pure Sk and hybrids with a large range of Sp admixture proportions
227	(0.1-0.9). 63 traits showed significant difference among groups (Figure 4b, Supplementary
228	Figure 12). In the vast majority of cases (50 traits), hybrid phenotypes were indistinguishable
229	from one of the parents, but differed from the other, suggesting dominance of one ancestral
230	background, consistent with some ecological separation of the backgrounds. In seven traits,
231	hybrid phenotypes were intermediate differing from both parents, indicative of an additive
232	contribution of both ancestral backgrounds. For six traits, hybrids exceeded phenotypic values
233	of both parents providing evidence for transgressive segregation. In all cases, the number of
234	significantly differentiated traits was found to be higher than under the null model (mean
235	number of significant traits after 10000 permutations: dominant Sk 4 +/- 2, dominant Sk 4 +/-

2, transgressive 0 +/- 0.3, intermediate 0 +/- 0.1; Supplementary Figure 13). Jeffares et al. 236 237 (2017) showed that for each trait the total proportion of phenotypic variance explained by the 238 additive genetic variance component (used as an estimated of the narrow-sense heritability) 239 ranged from 0 to around 90%. We found that across all 228 traits, considering Sp and Sk 240 ancestry components across the 1,925 genomic windows explained an equivalent amount of 241 phenotypic variance as all 172,935 SNPs segregating across all samples, being both highly correlated (Figure 4c, 4d; r = 0.82, *p*-value  $\leq 2.2 \cdot 10^{-16}$ ). Combinations of ancestral genetic 242 243 variation appear to be the main determinants of heritable phenotypic variation with only little 244 contribution from single-nucleotide mutations arising after admixture. In turn, this supports that the formation of hybrids is recent (see above), and few (adaptive) mutations have 245 246 occurred after it. 247 248 Ancestry also explained most of the variation in postzygotic reproductive isolation between 249 strains. Previous work revealed a negative correlation between spore viability and genome-250 wide SNP divergence between strains (Jeffares et al., 2015). The degree of similarity in 251 genome-wide ancestry had the same effect: the more dissimilar two strains were in their 252 ancestry, the lower the viability of the resulting spores (Figure 4e; Kendall correlation coefficients,  $\tau$ = -0.30, T= 259, p-value = 6.66  $\cdot$  10<sup>-3</sup>). This finding is consistent with 253 254 reproductive isolation being governed by many, genome-wide incompatibilities between the 255 Sp and Sk clade. Yet, in a number of cases spore survival was strongly reduced in strain 256 combinations with near-identical ancestry. In these cases, reproductive isolation may be 257 caused by few large effect mutations, including structural genomic changes that arose after

hybridization.

259



261 Structural genomic changes (structural variants or SVs hereafter) are candidates for large-262 effect mutations governing phenotypic variation (Küpper et al., 2016; Jeffares et al., 2017), 263 reproductive isolation (Hoffmann and Rieseberg, 2008; Teresa Avelar et al., 2013) and 264 heterospecific recombination (Ortiz-Barrientos et al., 2016). They may thus importantly 265 contribute to shaping heterogeneity in the distribution of ancestry blocks observed along the 266 genome (Jay et al., 2018; Poelstra et al., 2014) (Figure 2b). However, inference of SVs in 267 natural strains of fission yeast has been primary based on short-read sequencing (Jeffares et al., 268 2017). SV calls from short-read sequencing data are known to differ strongly by bioinformatic 269 pipeline, are prone to false positive inference and are limited in their ability to infer long-270 range SV, in particular in repetitive regions of the genome (Jeffares et al., 2017). 271 272 To obtain a reliable and comprehensive account of SV segregating across strains and test for a 273 possible association of SVs with the skewed ancestry in the genome, we generated 274 chromosome-level de novo genome assemblies for 17 of the most divergent samples using 275 single-molecule real time sequencing (mean sequence coverage 105x; Supplementary Table 276 7). For the purpose of methodological comparison, we also generated *de novo* assemblies for 277 a subset of 8 strains (including the reference Leupold's 972) based on nanopore sequencing 278 (mean sequence coverage: 140x). SVs were called using a mixed approach combining 279 alignment of *de novo* genomes and mapping of individual reads to the reference genome 280 (Wood et al., 2002). Both approaches and technologies yielded highly comparable results 281 (Methods, Supplementary Figure 14-17 and Supplementary Table 8). 282 283 After quality filtering, we retained a total of 832 variant calls including 563 insertions or 284 deletions (indels), 118 inversions, 110 translocations and 41 duplications. The 17 strains we 285 examined with long reads could be classified into six main karyotype arrangements (Figure

286	5a). The previously reported list of SVs of the same strains using short reads consisted of only
287	52 SVs (Jeffares et al., 2017) of which only 8 were found to overlap with the 832 calls from
288	long-read data. The vast majority of SVs were smaller than 10 kb (Figure 5b). The size
289	distribution was dominated by elements of 6 kb and 0.5 kb in length corresponding to known
290	transposable elements (TEs) and their flanking long terminal regions (LTRs), respectively
291	(Kelly and Levin, 2005). Only a small number of SVs corresponded to large-scale
292	rearrangements (50 kb - 2.2 Mb) including translocations between chromosomes (Figure 5a).
293	A subset of these have been characterized previously as large-effect modifiers of
294	recombination promoting reproductive isolation (Brown et al., 2011; Teresa Avelar et al.,
295	2013; Jeffares et al., 2017).
296	
297	Contrary to previous SV classification based on short reads (Jeffares et al., 2017), SV density
298	was not consistently increased in repetitive sequences such as centromeric and telomeric
299	regions illustrating the difficulty of short-read data in resolving SV in repetitive regions
300	(Figure 5c). Instead, we found that the frequency of SV was significantly elevated in close
301	proximity to developmentally programmed DNA double-strand breaks (DSB) associated with
302	recombination initiation (Fowler et al., 2014). The proportion of SV observed within [0, 0.5)
303	kb and [0.5, 1) kb of DSB was increased by 46% (p-value $<1x10^{-04}$ ) and 67% (p-
304	value<1x10 <sup>-04</sup> ) relative to random expectations. On the contrary, regions more distant than 10
305	kb from DSB were relatively depleted of SV (Supplementary Figure 18).
306	
307	Next, we imputed the ancestry of SV alleles from SNPs surrounding SV break points. We
308	calculated allele frequencies for SV in both ancestral clades and constructed a folded two-
309	dimensional site frequency spectrum (Figure 5d). The majority of variants (66 %) segregated
310	at frequencies below 0.3 in both ancestral genetic backgrounds. Very few SVs were

differentiated between ancestral populations (3 % of variants with frequency higher than 0.9 311 312 in one population and below 0.1 in the other). This pattern contrasted with the reference 313 spectrum derived from SNPs where the proportion of low frequency variants was similar at 314 60 %, but genetic differentiation between populations was substantially higher (21 % of SNP 315 variants with frequency higher than 0.9 in one population and below 0.1 in the other). The 316 difference was most pronounced for large SVs (larger than 10 kb) and TEs, for which we 317 estimated allele frequencies for all 57 strains by means of PCR and short-read data, 318 respectively. For TE's, 98 % of the total 1048 LTR variants segregated at frequencies below 319 0.3 in both ancestral populations without a single variant differentiating ancestral populations 320 (Figure 5d). Large SVs likewise segregated at low frequencies, being present at most in two 321 strains out of 57. This included the translocation reported for S. kambucha between 322 chromosome II and III (Zanders et al., 2014), which we found to be specific for that strain. 323 Only the large inversion on chromosome I segregated at higher frequency being present in 324 five strains out of 57, of which three were of pure Sp ancestry including the reference strain 325 (Supplementary Table 10). Additionally, SV segregating at high frequency (> 0.7) tended to 326 cluster in genomic regions with steep transitions in ancestry between Sp and Sk ancestry (p-327 value > 0.1; Supplementary Figure 19).

328

In summary, long-read sequencing provided a detailed account of species-wide diversity in structural genetic variation including over 800 high-quality variants ranging from small indels to large-scale inter-chromosomal rearrangements. SV calls showed substantial overlap among technologies (Pacific Biosciences, Nanopore) and approaches (de novo assembly vs. mapping), but less than 1 % of this variation was inferred from short-read data. This finding admonishes to caution when interpreting SV calls from short read data that is moreover sensitive to genotyping methods. In contrast to genome-wide SNPs, SVs segregated near-

exclusively at low frequencies and were rarely differentiated by ancestral origin. This is 336 337 consistent with strong diversity-reducing purifying selection relative to SNPs. The fact that 338 SVs, including large-scale rearrangements with known effects on recombination and 339 reproductive isolation (Brown et al., 2011; Teresa Avelar et al., 2013; Zanders et al., 2014), 340 were often unique to single strains precludes a role of SVs in shaping patterns of ancestral 341 heterospecific recombination. Moreover, while being concentrated in proximity to double-342 strand breaks, possibly due to improper repair upon recombination (Currall et al., 2013), SV were not significantly associated with steep transitions in ancestry blocks. Summarizing the 343 344 evidence, SV appears to have had little influence in shape genome-wide patterns of ancestral 345 admixture and cannot explain the prevalence of reproductive isolation as a function on 346 ancestral similarity (Figure 4e).

347

#### 348 Negative epistasis shapes the distribution of ancestral blocks

349 Alternatively, heterogeneity in the distribution and frequency of ancestry along the genome 350 may result from negative epistatic interactions of incompatible genetic backgrounds (Schumer 351 et al., 2016). An excess of homospecific combinations of physically distant loci can serve as 352 an indication of epistatic selection against genetic incompatibilities which can be segregating 353 at appreciable frequencies even within species (Corbett-Detig et al., 2013). We tested this 354 hypothesis by measuring ancestry disequilibrium (AD) between all possible pairs of genomic 355 windows within a chromosome. Specifically, we quantified linkage disequilibrium (LD) 356 between windows dominated by alleles from the same ancestral group (> 0.7) Sp-Sp or Sk-Sk 357 (reflecting positive AD) and contrasted it to the degree of linkage disequilibrium arising 358 between heterospecific allele combinations Sp-Sk (negative AD) (Supplementary Figure 20). 359 LD differed significantly between these two cases (Figure 6). While negative AD decreased rapidly with genetic distance ( $\mathbb{R}^2 < 0.2$  after 66, 19 and 21 kb respectively for each 360

361 chromosome) positive LD was higher in magnitude and extended over larger distances ( $\mathbb{R}^2 <$ 362 0.2 after 1.02, 0.54, and 0.18 Mb respectively for each chromosome in *Sk-Sk* comparisons and 363 1.59, 1.12, and 0.32 Mb for *Sp-Sp* comparisons). These results are consistent with a role of 364 epistatic selection during the course of hybridization shaping the ancestry composition of 365 admixed genomes.

366

# 367 **Discussion**

368 This study adds to the increasing evidence that hybridization plays an important role as a 369 rapid, 'creative' evolutionary force in natural populations (Seehausen, 2004; Mallet, 2007; 370 Soltis and Soltis, 2009; Abbott et al., 2013; Schumer et al., 2014; Abbott et al., 2016; Pennisi, 371 2016; Nieto Feliner et al., 2017). Recent heterospecific recombination between two ancestral 372 S. pombe populations shuffled genetic variation of genomes that diverged since classical 373 antiquity about 2,300 years ago. The timing of hybridization coincided with the onset of 374 intensified trans-continental human trade, suggesting an anthropogenic contribution. Several 375 samples showed similar distribution of ancestral blocks along the genome suggesting 376 comparable evolutionary histories, and allowing the identification of 8 discrete clusters. These 377 clusters, in general showed weak geographical grouping, initially interpreted as evidence for 378 reduced population structure with large recent world-wide gene flow (Jeffares et al., 2015). In 379 contrast, the world-wide distribution of the two ancestral linages suggests rapid and recent 380 global dispersion after hybridization followed by local differentiation. This study thus 381 highlights the importance of taking genomic non-independence into account. Allowing for the 382 fact that genomes are mosaics reflecting different evolutionary histories can fundamentally 383 alter inference on a species' evolutionary history.

384

385 Moreover, conceptualizing genetic variation as a function of ancestry blocks alternating along 386 the genome changes the view on adaptation. Admixture is significantly faster than 387 evolutionary change solely driven by mutation. Accordingly, phenotypic variation was near-388 exclusively explained by ancestry components with only little contribution from novel 389 mutations. Importantly, admixture not only filled the phenotypic space between parental 390 lineages, but also promoted transgressive segregation in several hybrids. This range of 391 phenotypic outcomes opens the opportunity for hybrids to enter novel ecological niches 392 (Nolte and Sheets, 2005; Pfennig et al., 2016) and track rapid environmental changes 393 (Eroukhmanoff et al., 2013).

394

395 Structural mutations have been described as prime candidates for rapid large-effect changes 396 with implications on phenotypic variation, recombination and reproductive isolation (Faria 397 and Navarro, 2010; Ortiz-Barrientos et al., 2016; Wellenreuther and Bernatchez, 2018). This 398 study contributes to this debate providing a detailed account of over 800 high-quality 399 structural variants identified across 17 chromosome level de novo genomes sampled from the 400 most divergent strains within the species. On the whole, SVs had little effect. While large-401 scale rearrangements in specific strains have been shown to affect fitness (Teresa Avelar et al., 402 2013; Nieuwenhuis et al., 2018) and promote reproductive isolation between specific strains 403 in S. pombe (Brown et al., 2011; Teresa Avelar et al., 2013), reproductive isolation was 404 overall best predicted by the degree of shared ancestry with little contribution from SVs. SVs 405 segregated at low frequencies in both ancestral populations and, contrary to what has been 406 suggested for specific genomic regions in other systems (Jay et al., 2018), they did not 407 account for genome-wide heterogeneity in introgression among strains during hybridization. 408 Much rather, analyses of ancestry disequilibrium suggest a role for negative epistasis between 409 multiple ancestry-specific loci spread across the genome rather than single major effect

- 410 mutations such as selfish elements or meiotic drivers (Zanders et al., 2014; Hu et al., 2017;
- 411 Nuckolls et al., 2017). Functional work is needed to identify the genetic elements conveying
- 412 reproductive isolation.
- 413

# 414 Material and Methods

- 415 Strains
- 416 This study is based on a global collection of *S. pombe* consisting of 161 world-wide
- 417 distributed strains (see **Supplementary Table 1**) described in Jeffares *et al.* (2015).
- 418

#### 419 Inferring ancestry components

- 420 To characterize genetic variation across all strains, we made use of publically available data in
- 421 variant call format (VCF) derived for all strains from Illumina sequencing with an average
- 422 coverage of around 80x (Jeffares et al., 2015). The VCF file consists of 172,935 SNPs
- 423 obtained after read mapping to the *S. pombe* 972 h<sup>-</sup> reference genome (ASM294v264) (Wood
- 424 et al., 2003) and quality filtering (see **Supplementary Table 1** for additional information).
- 425 We used a custom script in R 3.4.3 (Team, 2014) with the packages gdsfmt 1.14.1 and
- 426 SNPRelate 1.12.2 (Zheng et al., 2017, 2012), to divide the VCF file into genomic windows of
- 427 200 SNPs with overlap of 100 SNPs. This resulted in 1925 genomic windows of 1 89 kb in
- 428 length (mean 13 kb). For each window, we performed principal component analyses (PCA)
- 429 using *SNPRelate* 1.12.2 (Zheng et al., 2017, 2012) (example in Figure 1a and
- 430 **Supplementary Figure 1**). The proportion of variance explained by the major axis of
- 431 variation (PC1) was consistently high and allowed separating strains into two genetic
- 432 groups/clusters, Sp and Sk (see main text, Figure 1b). We calculated population genetic
- 433 parameters within clusters including pairwise nucleotide diversity ( $\pi$ ) (Nei and Li, 1979),
- 434 Watterson theta ( $\theta_w$ ) (Watterson, 1975), and Tajima's D (Tajima, 1989), as well as the

435 average number of pairwise differences between clusters  $(D_{xy})$  (Nei and Li, 1979) using 436 custom scripts. Statistical significance of the difference in nucleotide diversity ( $\pi$ ) between 437 ancestral clades was inferred using Kendall's  $\tau$  as test statistic. Since values of adjacent 438 windows are statistically non-independent due to linkage, we randomly subsampled 200 439 windows along the genome with replacement. This was repeated a total of 10 times for each 440 test statistic, and we report the maximum p-value. Given the consistent difference between 441 clusters (Figure 1 and Supplementary Figure 2, 3 and 5), normalised PC score could be 442 used to attribute either Sp (low-diversity) or Sk (high-diversity) ancestry to each window 443 (summary statistics for each window are given in Supplementary Table 2). This was 444 performed both for the subset of 57 samples (Figure 1c) and for all 161 samples 445 (Supplementary Figure 6). Using different window sizes (100, 50 and 40 SNPs with overlap of 50, 25 and 20 respectively) yielded qualitatively the same results. Intermediate values in 446 447 PC1 (between 0.25 and 0.75) were only observed in few, sequential windows where samples 448 transitioned between clusters (Supplementary Figure 3). The only exception was sample 449 JB1207, which we found to be diploid (for details see below). 450

#### 451 **Population structure after hybridization**

452 To characterise the genome-wide distribution of ancestry components along the genome, we 453 ran a hierarchical cluster analysis on the matrix containing ancestry information (Sp or Sk) for 454 each window (columns) and strain (rows) using the R package Pvclust 2.0.0 (Suzuki and 455 Shimodaira, 2006). Pvclust includes a multiscale bootstrap resampling approach to calculate 456 approximately unbiased probability values (p-values) for each cluster. We specified 1000 457 bootstraps using the Ward method and a Euclidian-based dissimilarity matrix. The analysis 458 was run both for the whole genome (Figure 1c) and by chromosome (Figure 1c, 459 Supplementary Figure 7).

460

#### 461 Phylogenetic analysis of the mitochondrial genome

- 462 From the VCF file, we extracted mitochondrial variants for all 161 samples (Jeffares et al.,
- 463 2015) and generated an alignment in *fasta* format by substituting SNPs into the reference S.
- 464 *pombe* 972 h- reference genome (ASM294v264) using the package *vcf2fasta*
- 465 (https://github.com/JoseBlanca/vcf2fasta/, version Nov. 2015). We excluded variants in
- 466 mitochondrial regions with SVs inferred from long reads. A maximum likelihood tree was
- 467 calculated using *RaxML* (version 8.2.10-gcc-mpi) (Stamatakis, 2014) with default parameters,
- 468 GTRGAMMAI approximation, final optimization with GTR + GAMMA + I and 1000
- 469 bootstraps. The final tree was visualised using *FigTree* 1.4.3
- 470 (http://tree.bio.ed.ac.uk/software/figtree/) (Supplementary Figure 8).

471

#### 472 Time of hybridization

473 Previous work (Jeffares et al., 2015) has shown that the time to the most recent common 474 ancestor for 161 samples dates back to around 2300 years ago. This defines the maximum 475 boundary for the time of hybridization. We used the theoretical model by Janzen et al., (2018) 476 to infer the age of the initial hybridization event. The model predicts the number of ancestry 477 blocks and junctions present in a hybrid individual as a function of time and effective 478 population size  $(N_e)$ . First, we obtained an estimate of  $N_e$  using the multiple sequential 479 Markovian coalescent (MSMC). We constructed artificial diploid genomes from strains with 480 consistent clustering by ancestry (Figure 1c) and estimated change in  $N_e$  as function across 481 time using MSMC 2-2.0.0 (Schiffels and Durbin, 2014). In total we took four samples per 482 group and produced diploid genomes in all possible six pairs for each group, except for one 483 cluster that had only two samples (JB1205 and JB1206). Bootstraps were produced for each 484 analysis, subsampling 25 genomic fragments per chromosome of 200 kb each. Resulting

485	effective population size and time was scaled using reported mutation rate of $2 \cdot 10^{-10}$
486	mutations site <sup>-1</sup> generation <sup>-1</sup> (Farlow et al., 2015). Although it is difficult to be certain of the
487	number of independent hybridization events, it is interesting to see that some clusters show
488	similar demographic histories (Supplementary Figure 21). Regardless of the demographic
489	history in each cluster, long-term $N_e$ as estimated by the harmonic mean ranged between 1 $\cdot$
490	10 <sup>5</sup> and 1 $\cdot$ 10 <sup>9</sup> . $N_e$ of the near-pure ancestral Sp and Sk cluster was 7 $\cdot$ 10 <sup>5</sup> and 9 $\cdot$ 10 <sup>6</sup> ,
491	respectively. These estimates of $N_e$ are consistent with previous reports of $1 \cdot 10^7$ (Farlow et
492	al., 2015).
493	We then used a customised R script with the ancestral component matrix to estimate the
494	number of ancestry blocks (Sp or Sk clade) (Supplementary Figure 10). We used the R script
495	from Janzen et al., (2018), and ran the model in each sample and chromosome using: $N_e = 1$ .
496	10 <sup>6</sup> , $r =$ number of genomic windows per chromosome, $h0 = 0.298$ (mean heterogenicity ( $h0$ )
497	was estimated from the ancestral haplotype matrix) and $c = 7.1, 5.6, and 4.1$ respectively for
498	chromosome I, II and III (values taken from Munz et al. (1989)) (Supplementary Figure 11).
499	Given the large $N_e$ , no changes in mean heterogenicity is expected over time after
500	hybridization due to drift (the proportion of ancestral haplotypes $Sp$ and $Sk$ in hybrids,
501	estimated as $2pq$ , where p and q are the proportion of each ancestral clade in hybrids).
502	Accordingly, results did not change within the range of the large $N_e$ values. For this analysis,
503	samples with proportion of admixture lower than 0.1 were excluded.
504	

# 505 Phenotypic variation and reproductive isolation

We sourced phenotypic data of 229 phenotypic measurements in the 161 strains including
amino acid quantification on liquid chromatography (aaconc), growth and stress on solid
media (smgrowth), cell growth parameters and kinetics in liquid media (lmgrowth) and cell

509 morphology (shape1 and shape2) from Jeffares et al. (2015). Data on reproductive isolation

510	measured as the percentage of viable spores in pairs of crosses were compiled from Jeffares et
511	al. (2015) and Marsellach (2017). A summary of all phenotypic measurements and
512	reproductive data is provided in <b>Supplementary Table 4</b> and <b>5</b> , respectively.
513	
514	First, we normalized each phenotypic trait y using rank-based transformation with the
515	relationship normal.y = qnorm( rank ( $y$ ) / (1 + length( $y$ ))). We then conducted PCA on
516	normalized values of all phentoypic traits using the R package missMDA 1.12 (Josse and
517	Husson, 2016). We estimated the number of dimensions for the principal component analysis
518	by cross-validation, testing up to 30 PC components and imputing missing values. In addition
519	to PCA decomposing variance across all traits, we examined the effect of admixture on each
520	trait separately. Samples were divided into three discrete categories of admixture: two groups
521	including samples with low admixture proportions (proportion of $Sp$ or $Sk$ clades higher than
522	0.9), and one for hybrid samples (proportion of $Sp$ or $Sk$ clades between 0.1 to 0.9).
523	Significant differences in phenotypic distributions between groups were tested using <i>Tukey</i>
524	Honest Significant Differences as implemented in Stats 3.4.2 (Team, 2014). Supplementary
525	Figure 12 shows the distribution of phenotypic values by admixture category for each trait.
526	The number of traits with significant differences among groups was contrasted to values
527	obtained by randomising admixture categories without replacement (permutations of the Sp,
528	Sk, or hybrid category). Observed values were contrasted with distribution of the expected
529	number of significant traits after running 10000 independent permutations (Supplementary
530	Figure 13).
531	
532	Heritability

533 Heritability was estimated for all normalized traits using LDAK 5.94 (Speed et al., 2012),

calculating independent kinship matrices derived from: 1) all SNPs and 2) ancestral

haplotypes. Both SNPs and haplotype data were binary encoded (0 or 1). Jeffares et al. (2015) showed that heritability estimates between normalised and raw values are highly correlated (r= 0.69, p-value  $\leq 2.2 \cdot 10^{-16}$ ). Heritability estimated with SNP values were strongly correlated with those from ancestral haplotypes (r = 0.82, p-value  $\leq 2.2 \cdot 10^{-16}$ ). Heritability estimates and standard deviation for each trait for both SNP and ancestral haplotypes are detailed in **Supplementary Table 6**.

541

# 542 Identification of ploidy changes

543 S. pombe is generally considered haploid under natural conditions. Yet, for two samples 544 ancestry components did not separate on the principle component axis 1 (see above) for much 545 of the genome. Instead, these samples were intermediate in PC1 score. A possible explanation 546 is diploidisation of the two ancestral genomes. To establish the potential ploidy of samples, 547 we called variants for all 161 samples using the Illumina data from Jeffares et al (2015). 548 Cleaned reads were mapped with BWA (version 0.7.17-r1188) in default settings and variants 549 were called using samtools and bcftools (version 1.8). After filtering reads with a QUAL 550 score > 25, the number of heterozygous sites per base per 20kb window were calculated. 551 Additionally the nuclear content (C) as measured by Jeffares et al. (2015) (Supplementary 552 Table S4 in Jeffares et al (2015)) were used to verify increased ploidy. Two samples showed 553 high heterozygosity along the genome (JB1169 and JB1207) of which JB1207 for which data 554 were available also showed a high C-value, suggesting that these samples are diploid 555 (Supplementary Figures 4 & 22). In JB1207, heterozygosity varies along the genome, with 556 regions of high and low diversity. Assigning ancestry (see **Supplementary Figure 6**), shows 557 that the haploid parents differed from each other and that both chromosomes stem from 558 hybrids between the Sp and Sk clades. Sample JB1110 showed genomic content similar to

JB1207, but did not show heterozygosity levels above that of haploid strains, suggesting theincrease in genome content occurred by autoploidization.

561

# 562 High-weight genomic DNA extraction and whole genome sequencing

563 To obtain high weight gDNA for long-read sequencing, we grew strains from single colonies 564 and cultured them in 200 mL liquid EMM at 32 °C shaking at 150 r.p.m. overnight. Standard media and growth conditions were used throughout this work (Hagan et al., 2016) with minor 565 566 modifications: We used standard liquid Edinburgh Minimal Medium (EMM; Per liter: 567 Potassium Hydrogen Phthalate 3.0 g, Na HPO<sub>4</sub>·2H<sub>2</sub>O 2.76 g, NH<sub>4</sub>Cl 5.0 g, D-glucose 20 g, 568 MgCl<sub>2</sub>·6H2O 1.05 g, CaCl<sub>2</sub>·2H<sub>2</sub>O 14.7 mg, KCl 1 g, Na<sub>2</sub>SO<sub>4</sub> 40 mg, Vitamin Stock ×1000 1.0 ml, Mineral Stock  $\times 10,000$  0.1 ml, supplemented with 100 mg l<sup>-1</sup> adenine and 225 mg l<sup>-1</sup> 569 leucine) for the asexual growth. DNA extraction was performed with Genomic Tip 500/G or 570 571 100/G kits (Qiagen) following the manufacturer's instruction, but using Lallzyme MMX for lysis (Flor-Parra et al 2014, doi:10.1002/yea.2994). For each sample, 20 kb libraries were 572 573 produced that were sequenced on one SMRT cell per library using the Pacific Biosciences 574 RSII Technology Platform (PacBio®, CA). For a subset of eight samples, additional 575 sequencing was performed using Oxford Nanopore (MinION). Sequencing was performed at 576 SciLifeLab, Uppsala, Gene centre LMU, Munich and The Genomics & Bioinformatics 577 Laboratory, University of York. We obtained on average 80x (SMRT) and 140x (nanopore) 578 coverage for the nuclear genome for each sample (summary in **Supplementary Table 7**). 579 580 Additionally, 2.5 µg of the same DNA was delivered to the SNP&SEQ Technology Platform 581 at the Uppsala Biomedical Centre (BMC), for Illumina sequencing. Libraries were prepared

using the TruSeq PCRfree DNA library preparation kit (Illumina Inc.). Sequencing was

583 performed on all samples pooled into a single lane, with cluster generation and 150 cycles

584 paired-end sequencing on the HiSeqX system with v2.5 sequencing chemistry (Illumina Inc.).

585 These data were used for draft genome polishing (see below).

586

#### 587 De novo assembly of single-molecule read data

588 *De novo* genomes were assembled with *Canu* 1.5 (Koren et al., 2017) using default

parameters. BridgeMapper from the *SMRT* 2.3.0 package was used to polish and subsequently

assess the quality of genome assembly. Draft genomes were additionally polishing using short

591 Illumina reads, running four rounds of read mapping to the draft genome with *BWA* 0.7.15

and polishing with *Pilon* 1.22 (Walker et al., 2014). Summary statistics of the final assembled

593 genomes are found in **Supplementary Table 7**. *De novo* genomes were aligned to the

reference genome using *MUMmer* 3.23 (Kurtz et al., 2004). Contigs were classified by

reference chromosome to which they showed the highest degree of complementary. We used

596 customised python scripts to identify and trim mitochondrial genomes.

597

#### 598 Structural variant detection

599 Structural variants (SVs) were identified by a combination of a *de novo* and mapping 600 approach. De novo genomes were aligned to the reference genome using MUMmer, and SVs 601 were called using the function show-diff and the package SVMU 0.2beta (Khost et al., 2016). 602 Then, raw long reads were mapped to the reference genome with *NGMLR* and genotypes were 603 called using the package *Sniffles* (Sedlazeck et al., 2018). We implemented a new function 604 within Sniffles "forced genotypes", which calls SVs by validating the mapping calls from an 605 existing list of breaking points or SVs. This reports the read support per variant even down to 606 a single read. We forced genotypes using the list of *de novo* breaking points to generate a 607 multi-sample VCF file. SVs were merged using the package SURVIVOR (Jeffares et al., 2017) 608 option merge with a threshold of 1kbp and requiring the same type. In total, it resulted in a list

609 of 1498 SVs with 892 in common between the mapping and *de-novo* approaches

# 610 (Supplementary Figure 14).

612	Within the 892 common variants we compared the accuracy of genotyping between sample by
613	comparing genotypes obtained from <i>de novo</i> genomes and by mapping reads to reference
614	genome. Additionally, we compared genotypes in samples sequenced with both PacBio and
615	MinIon. In total we sequenced 8 samples with both technologies. We found high consistency
616	for variants called with both sequencing technologies and observed that allele frequencies
617	were highly correlated (r = 0.98, p-value $\leq 2.2 \times 10^{-16}$ ) (Supplementary Figures 14 - 17).
618	Only common SVs between the mapping and <i>de-novo</i> approach were considered, and variants
619	with consistency below 50% were removed. We manually checked large SVs (larger than
620	10kb) by comparing the list of SVs with the alignment of the <i>de novo</i> genomes to the
621	reference genome from MUMmer. This resulted in a final data set with 832 SVs
622	(Supplementary Table 8).
623	
623 624	Distribution of SVs around developmentally programmed DNA double-strand breaks
	Distribution of SVs around developmentally programmed DNA double-strand breaks (DSB)
624	
624 625	(DSB)
624 625 626	(DSB) We tested the association between DSB and SVs by comparing the physical genomic
624 625 626 627	<ul><li>(DSB)</li><li>We tested the association between DSB and SVs by comparing the physical genomic coordinates of the final list of SV with DSB locations accessed from Fowler et al., (2014).</li></ul>
624 625 626 627 628	<ul> <li>(DSB)</li> <li>We tested the association between DSB and SVs by comparing the physical genomic coordinates of the final list of SV with DSB locations accessed from Fowler et al., (2014).</li> <li>Maintaining the same number of SV per chromosome, we used a customized R script to</li> </ul>
624 625 626 627 628 629	(DSB) We tested the association between DSB and SVs by comparing the physical genomic coordinates of the final list of SV with DSB locations accessed from Fowler et al., (2014). Maintaining the same number of SV per chromosome, we used a customized R script to randomise SV coordinates and measure the distances to the closest DSB. We counted the
624 625 626 627 628 629 630	(DSB) We tested the association between DSB and SVs by comparing the physical genomic coordinates of the final list of SV with DSB locations accessed from Fowler et al., (2014). Maintaining the same number of SV per chromosome, we used a customized R script to randomise SV coordinates and measure the distances to the closest DSB. We counted the number of SV present within different intervals of physical genetic distance ([0,500), [500,

observed values were obtained from the fraction of expected values higher than the observed
value from the original data (Supplementary Figures 18).

636

# 637 PCR validation of large SVs

To test the frequency of large inversions and rearrangements observed from long read data, we performed PCR verification over the breakpoints in the 57 non-clone samples. PCR was performed for both sides of the breakpoints, with a combination of one primer 'outside' of the inversion and both primers 'inside' the inversion (**Supplementary Figure 23**). PCR were performed on DNA using standard *Taq* polymerase, with annealing temperature at 59°C. The primers used, the coordinates in the reference and the expected amplicon length are given in **Supplementary Table 9**.

645

# 646 Distribution of structural variants in ancestral population – Two dimensional folded site 647 frequency spectrum

648 We used the location of break points of SVs to identify whether a variant was located in the 649 Sp or Sk genetic background in each sample. Ancestral haplotypes are difficult to infer in 650 telomeric and centromeric regions given the low confidence in SNP calling in those regions, 651 resulting in low percentage of variance explained by PC1. Thus SVs with break points in 652 those regions were excluded from this analysis (19 SVs). SVs were grouped by ancestral 653 group and allele frequencies were calculated for each ancestral population. We used these 654 frequencies to build a two dimensional folded site frequency spectrum (2dSFS). In order to 655 compare this 2dSFS, we repeated the analysis using SNP data from all 57 samples. 656 Considering that the majority of identified SVs with long reads were transposable elements, 657 we also made use of LRT insertion-deletion polymorphism (indels) inferred from short reads. For this additional data we produced a similar folded 2d SFS. LTR indel data were taken from
Jeffares et al., (2015) and are listed in Supplementary Table 11.

660

# 661 **Decay in linkage disequilibrium (LD)**

To contrast LD between alleles from alternative ancestral groups, we calculated LD between all described genomic windows within chromosomes (**Supplementary Figure 20**). For this analysis only hybrid samples were considered (strains with admixture proportion higher than 0.1). For each pair of windows, we polarized windows by ancestry (at a threshold of > 0.7) and calculated standardized LD as the squared Pearson's correlation coefficient ( $R^2$ ) (Hill and Robertson, 1968; Weir, 1979). This measurement takes into consideration difference in allele frequencies. The expected value of  $R^2$  (E( $R^2$ )) can be approximated by (Hill and Weir, 1988):

669 
$$E(R^2) = \left(\frac{10+C}{(2+C)*(11+C)}\right) * \left(1 + \frac{(3+C)*(12+12C+C^2)}{n*(2+C)*(11+C)}\right)$$

670 Where C corresponds to product between the genetic distance (bp) and the population 671 recombination rate ( $\rho$ ) in n number of haplotype sampled. The population recombination rate was calculated as:  $\rho = 4 * N_e * c$ , where c is the recombination fraction between sites and Ne 672 is the effective population size. We fitted a nonlinear model to obtain least squares estimates 673 674 of p using a customized R script. The decay of LD with physical distance can be described 675 with this model (Remington et al., 2001). LD values were grouped in three categories: i) comparison between windows with high proportion (Sp>0.7) of Sp ancestral group (Sp-Sp); ii) 676 high proportion (Sk>0.7) of Sk ancestral group (Sk-Sk); and iii) high proportion of opposite 677 678 ancestral groups (Sp-Sk). i) and ii) represent cases of positive ancestry disequilibrium, iii) will 679 be denoted as negative ancestry disequilibrium.

680

#### 681 Data availability

Nanopore, single-molecule real time sequencing data and de-novo genomes are available at
NCBI Sequence Read Archive, BioProject ID XXX.

684

686

#### 685 Acknowledgments

We thank Fidel Botero-Castro, Ana Catalán, Sebastian Höhna, Ulrich Knief, Claire Peart, 687 688 Joshua Peñalba, Ricardo Pereira, Matthias Weissensteiner, (LMU Munich) and S. Lorena 689 Ament-Velásquez (Uppsala University) for providing valuable intellectual input on the 690 various analyses, sharing scripts and critically comment on the manuscript. We are further 691 indebted to Bernadette Weissensteiner for extensive help with laboratory work and Saurabh 692 Pophaly for bioinformatics support (LMU Munich). We further acknowledge support for data 693 generation from the National Genomics Infrastructure, Uppsala, Sweden, the Gene Centre, 694 Munich, Germany, Sally James and Peter Ashton from the Bioscience Technology Facility, 695 Department of Biology, University of York, U.K, and James Chong, Department of Biology, 696 University of York, U.K. The computational infrastructure was provided by the UPPMAX Next-Generation Sequencing Cluster and Storage (UPPNEX) project funded by the Knut and 697 698 Alice Wallenberg Foundation and the Swedish National Infrastructure for Computing and the 699 York Advanced Research Computing Cluster (YARCC), University of York, U.K. This study 700 was funded by LMU Munich to JW and NHGRI UM1 HG008898 to FS.

701

# 702 Contributions

ST, BN, DJ and JW conceived of the study; All analyses were performed by ST with contributions from FS in structural variation calling, JD in de novo assembly, BN in ancestral inference and population genetics parameters and DJ in phenotypic and heritability analyses; ST and JD assembled de-novo genomes; BN designed primers for PCR validation of structural variants; ST, BN, and JW wrote the manuscript with input from all other authors.

708

#### 709 Competing Interests statement

710 The authors declare no competing interests.

# 711712 References

7	1	2
1	т	5

714 Abbott, R., Albach, D., Ansell, S., Arntzen, J.W., Baird, S.J.E., Bierne, N., Boughman, J., 715 Brelsford, A., Buerkle, C.A., Buggs, R., Butlin, R.K., Dieckmann, U., Eroukhmanoff, 716 F., Grill, A., Cahan, S.H., Hermansen, J.S., Hewitt, G., Hudson, A.G., Jiggins, C., 717 Jones, J., Keller, B., Marczewski, T., Mallet, J., Martinez-Rodriguez, P., Möst, M., 718 Mullen, S., Nichols, R., Nolte, A.W., Parisod, C., Pfennig, K., Rice, A.M., Ritchie, 719 M.G., Seifert, B., Smadja, C.M., Stelkens, R., Szymura, J.M., Väinölä, R., Wolf, 720 J.B.W., Zinner, D., 2013. Hybridization and speciation. J. Evol. Biol. 26, 229–246. 721 https://doi.org/10.1111/j.1420-9101.2012.02599.x 722 Abbott, R.J., Barton, N.H., Good, J.M., 2016. Genomics of hybridization and its evolutionary 723 consequences. Mol. Ecol. 25, 2325–2332. https://doi.org/10.1111/mec.13685 724 Brown, W.R.A., Liti, G., Rosa, C., James, S., Roberts, I., Robert, V., Jolly, N., Tang, W., 725 Baumann, P., Green, C., Schlegel, K., Young, J., Hirchaud, F., Leek, S., Thomas, G., Blomberg, A., Warringer, J., 2011. A Geographically Diverse Collection of 726 Schizosaccharomyces pombe Isolates Shows Limited Phenotypic Variation but 727 728 Extensive Karyotypic Diversity. G3 GenesGenomesGenetics 1, 615–626. 729 https://doi.org/10.1534/g3.111.001123 Corbett-Detig, R.B., Zhou, J., Clark, A.G., Hartl, D.L., Ayroles, J.F., 2013. Genetic 730 731 incompatibilities are widespread within species. Nature 504, 135–137. 732 https://doi.org/10.1038/nature12678 733 Currall, B.B., Chiangmai, C., Talkowski, M.E., Morton, C.C., 2013. Mechanisms for 734 Structural Variation in the Human Genome. Curr. Genet. Med. Rep. 1, 81–90. 735 https://doi.org/10.1007/s40142-013-0012-8 736 Dowling, T. E., Smith, G. R. & Brown, W. M. Reproductive isolation and introgression 737 between Notropis cornutus and Notropis chrysocephalus (family Cyprinidae): 738 comparison of morphology, allozymes, and mitochondrial DNA. Evolution. 43, 620-739 634 (1989). 740 Eroukhmanoff, F., Hermansen, J.S., Bailey, R.I., Sæther, S.A., Sætre, G.-P., 2013. Local 741 adaptation within a hybrid species. Heredity 111, 286–292. 742 https://doi.org/10.1038/hdy.2013.47 743 Faria, R., Navarro, A., 2010. Chromosomal speciation revisited: rearranging theory with 744 pieces of evidence. Trends Ecol. Evol. 25, 660-669. 745 https://doi.org/10.1016/j.tree.2010.07.008 746 Farlow, A., Long, H., Arnoux, S., Sung, W., Doak, T.G., Nordborg, M., Lynch, M., 2015. The 747 Spontaneous Mutation Rate in the Fission Yeast Schizosaccharomyces pombe. 748 Genetics 201, 737–744. https://doi.org/10.1534/genetics.115.177329 749 Fawcett, J.A., Iida, T., Takuno, S., Sugino, R.P., Kado, T., Kugou, K., Mura, S., Kobayashi, T., Ohta, K., Nakayama, J., Innan, H., 2014. Population Genomics of the Fission 750 751 Yeast Schizosaccharomyces pombe. PLOS ONE 9, e104241. 752 https://doi.org/10.1371/journal.pone.0104241 753 Fisher, R.A., 1999. The genetical theory of natural selection: a complete variorum edition. 754 Oxford University Press. Fowler, K.R., Sasaki, M., Milman, N., Keeney, S., Smith, G.R., 2014. Evolutionarily diverse 755 756 determinants of meiotic DNA break and recombination landscapes across the genome. 757 Genome Res. 24, 1650–1664. https://doi.org/10.1101/gr.172122.114 758 Hagan, I.M., Carr, A.M., Grallert, A., Nurse, P., 2016. Fission yeast: a laboratory manual. 759 Cold Spring Harbor Laboratory Press.

- Hill, W.G., Robertson, A., 1968. Linkage disequilibrium in finite populations. Theor. Appl.
   Genet. 38, 226–231. https://doi.org/10.1007/BF01245622
- Hill, W.G., Weir, B.S., 1988. Variances and covariances of squared linkage disequilibria in
  finite populations. Theor. Popul. Biol. 33, 54–78. https://doi.org/10.1016/00405809(88)90004-4
- Hoffman, C.S., Wood, V., Fantes, P.A., 2015. An Ancient Yeast for Young Geneticists: A
  Primer on the Schizosaccharomyces pombe Model System. Genetics 201, 403–423.
  https://doi.org/10.1534/genetics.115.181503
- Hoffmann, A.A., Rieseberg, L.H., 2008. Revisiting the Impact of Inversions in Evolution:
  From Population Genetic Markers to Drivers of Adaptive Shifts and Speciation? Annu.
  Rev. Ecol. Evol. Syst. 39, 21–42.
- 771 https://doi.org/10.1146/annurev.ecolsys.39.110707.173532
- Hu, W., Jiang, Z.-D., Suo, F., Zheng, J.-X., He, W.-Z., Du, L.-L., 2017. A large gene family
  in fission yeast encodes spore killers that subvert Mendel's law. eLife 6.
  https://doi.org/10.7554/eLife.26057
- Janzen, T., Nolte, A. W. & Traulsen, A. The breakdown of genomic ancestry blocks in hybrid lineages given a finite number of recombination sites: breakdown of ancestry blocks after hybridization. *Evolution*. **72**, 735–750 (2018).
- Jay, P., Whibley, A., Frézal, L., Rodríguez de Cara, M.Á., Nowell, R.W., Mallet, J.,
  Dasmahapatra, K.K., Joron, M., 2018. Supergene Evolution Triggered by the
  Introgression of a Chromosomal Inversion. Curr. Biol. 28, 1839-1845.e3.
  https://doi.org/10.1016/j.cub.2018.04.072
- Jeffares, D.C., 2018. The natural diversity and ecology of fission yeast. Yeast 35, 253–260.
   https://doi.org/10.1002/yea.3293
- Jeffares, D.C., Jolly, C., Hoti, M., Speed, D., Shaw, L., Rallis, C., Balloux, F., Dessimoz, C.,
  Bähler, J., Sedlazeck, F.J., 2017. Transient structural variations have strong effects on
  quantitative traits and reproductive isolation in fission yeast. Nat. Commun. 8, 14061.
  https://doi.org/10.1038/ncomms14061
- Jeffares, D.C., Rallis, C., Rieux, A., Speed, D., Převorovský, M., Mourier, T., Marsellach,
  F.X., Iqbal, Z., Lau, W., Cheng, T.M.K., Pracana, R., Mülleder, M., Lawson, J.L.D.,
  Chessel, A., Bala, S., Hellenthal, G., O'Fallon, B., Keane, T., Simpson, J.T., Bischof,
- 791 L., Tomiczek, B., Bitton, D.A., Sideri, T., Codlin, S., Hellberg, J.E.E.U., van Trigt, L.,
- 792 Jeffery, L., Li, J.-J., Atkinson, S., Thodberg, M., Febrer, M., McLay, K., Drou, N.,
- Brown, W., Hayles, J., Salas, R.E.C., Ralser, M., Maniatis, N., Balding, D.J., Balloux,
- F., Durbin, R., Bähler, J., 2015. The genomic and phenotypic diversity of
- 795Schizosaccharomyces pombe. Nat. Genet. 47, 235–241.
- 796 https://doi.org/10.1038/ng.3215
- Josse, J., Husson, F., 2016. missMDA: A Package for Handling Missing Values in
   Multivariate Data Analysis. J. Stat. Softw. 70. https://doi.org/10.18637/jss.v070.i01
- Kelly, F.D., Levin, H.L., 2005. The evolution of transposons in *Schizosaccharomyces pombe*.
  Cytogenet. Genome Res. 110, 566–574. https://doi.org/10.1159/000084990
- Khost, D. E., Eickbush, D. G. & Larracuente, A. M. Single molecule long read sequencing
   resolves the detailed structure of complex satellite DNA loci in. (2016).
- Kondrat'eva, V.I., Naumov, G.I., 2001. The Phenomenon of Spore Killing in
  Schizosaccharomyces pombe Hybrids. Dokl. Biol. Sci. 379, 385–388.
  https://doi.org/10.1023/A:1011624918673
- Koren, S., Walenz, B.P., Berlin, K., Miller, J.R., Bergman, N.H., Phillippy, A.M., 2017.
  Canu: scalable and accurate long-read assembly via adaptive *k* -mer weighting and
  repeat separation. Genome Res. 27, 722–736. https://doi.org/10.1101/gr.215087.116

809	Küpper, C., Stocks, M., Risse, J.E., dos Remedios, N., Farrell, L.L., McRae, S.B., Morgan,
810	T.C., Karlionova, N., Pinchuk, P., Verkuil, Y.I., Kitaysky, A.S., Wingfield, J.C.,
811	Piersma, T., Zeng, K., Slate, J., Blaxter, M., Lank, D.B., Burke, T., 2016. A supergene
812	determines highly divergent male reproductive morphs in the ruff. Nat. Genet. 48, 79–
813	83.
814	Kurtz, S., Phillippy, A., Delcher, A.L., Smoot, M., Shumway, M., Antonescu, C., Salzberg,
815	S.L., 2004. Versatile and open software for comparing large genomes. Genome Biol. 5,
816	R12.
817	Lamichhaney, S. et al. Rapid hybrid speciation in Darwin's finches. Science eaao4593 (2017).
818	Leducq, JB., Nielly-Thibault, L., Charron, G., Eberlein, C., Verta, JP., Samani, P.,
819	Sylvester, K., Hittinger, C.T., Bell, G., Landry, C.R., 2016. Speciation driven by
820	hybridization and chromosomal plasticity in a wild yeast. Nat. Microbiol. 1, 15003.
821	https://doi.org/10.1038/nmicrobiol.2015.3
822	Mallet, J., 2007. Hybrid speciation. Nature 446, 279–283.
823	https://doi.org/10.1038/nature05706
824	Mallet, J., 2005. Hybridization as an invasion of the genome. Trends Ecol. Evol. 20, 229–237.
825	Marsellach, X. A non-genetic meiotic repair program inferred from spore survival values in
826	fission yeast wild isolates: a clue for an epigenetic ratchet-like model of ageing?
827	(2017).
828	McDonald, M.J., Rice, D.P., Desai, M.M., 2016. Sex speeds adaptation by altering the
829	dynamics of molecular evolution. Nature 531, 233–236.
830	https://doi.org/10.1038/nature17143
831	Meier, J.I., Marques, D.A., Mwaiko, S., Wagner, C.E., Excoffier, L., Seehausen, O., 2017.
832	Ancient hybridization fuels rapid cichlid fish adaptive radiations. Nat. Commun. 8,
833	ncomms14363. https://doi.org/10.1038/ncomms14363
834	Muller, H.J., 1932. Some genetic aspects of sex. Am. Nat. 66, 118–138.
835	Munz, P., Wolf, K., Kohli, J., Leupold, U., 1989. Genetics overview. Mol. Biol. Fission Yeast
836	1–30.
837	Naumov, G.I., Kondratieva, V.I., Naumova, E.S., 2015. Hybrid sterility of the yeast
838	Schizosaccharomyces pombe: Genetic genus and many species in statu nascendi?
839	Microbiology 84, 159–169. https://doi.org/10.1134/S0026261715010099
840	Nei, M., Li, W.H., 1979. Mathematical model for studying genetic variation in terms of
841	restriction endonucleases. Proc. Natl. Acad. Sci. 76, 5269–5273.
842	https://doi.org/10.1073/pnas.76.10.5269
843	Nieto Feliner, G., Álvarez, I., Fuertes-Aguilar, J., Heuertz, M., Marques, I., Moharrek, F.,
844	Piñeiro, R., Riina, R., Rosselló, J.A., Soltis, P.S., Villa-Machío, I., 2017. Is homoploid
845	hybrid speciation that rare? An empiricist's view. Heredity 118, 513–516.
846	https://doi.org/10.1038/hdy.2017.7
847	Nieuwenhuis, B.P.S., Tusso, S., Bjerling, P., Stångberg, J., Wolf, J.B.W., Immler, S., 2018.
848	Repeated evolution of self-compatibility for reproductive assurance. Nat. Commun. 9.
849	https://doi.org/10.1038/s41467-018-04054-6
850	Nolte, A.W., Sheets, H.D., 2005. Shape based assignment tests suggest transgressive
851	phenotypes in natural sculpin hybrids (Teleostei, Scorpaeniformes, Cottidae). Front.
852	Zool. 2, 11. https://doi.org/10.1186/1742-9994-2-11
853	Nuckolls, N.L., Bravo Núñez, M.A., Eickbush, M.T., Young, J.M., Lange, J.J., Yu, J.S.,
854	Smith, G.R., Jaspersen, S.L., Malik, H.S., Zanders, S.E., 2017. wtf genes are prolific
855	dual poison-antidote meiotic drivers. eLife 6. https://doi.org/10.7554/eLife.26033
856	Ortiz-Barrientos, D., Engelstädter, J., Rieseberg, L.H., 2016. Recombination Rate Evolution
857	and the Origin of Species. Trends Ecol. Evol. 31, 226–236.
858	https://doi.org/10.1016/j.tree.2015.12.016

- Payseur, B. A. & Rieseberg, L. H. A genomic perspective on hybridization and speciation.
   *Mol. Ecol.* n/a-n/a (2016).
- Pennisi, E., 2016. A shortcut to a species. Science 354, 818–818.
   https://doi.org/10.1126/science.354.6314.818
- Peter, J., De Chiara, M., Friedrich, A., Yue, J.-X., Pflieger, D., Bergström, A., Sigwalt, A.,
  Barre, B., Freel, K., Llored, A., Cruaud, C., Labadie, K., Aury, J.-M., Istace, B.,
  Lebrigand, K., Barbry, P., Engelen, S., Lemainque, A., Wincker, P., Liti, G.,
- Schacherer, J., 2018. Genome evolution across 1,011 Saccharomyces cerevisiae
  isolates. Nature 556, 339–344. https://doi.org/10.1038/s41586-018-0030-5
- Pfennig, K.S., Kelly, A.L., Pierce, A.A., 2016. Hybridization as a facilitator of species range
  expansion. Proc. R. Soc. B Biol. Sci. 283, 20161329.
  https://doi.org/10.1098/rspb.2016.1329
- Poelstra, J.W., Vijay, N., Bossu, Christen, Lantz, Henrik, Ryll, Bettina, Müller, Inge,
  Baglione, Vittorio, Unneberg, Per, Wikelski, Martin, Grabherr, Manfred, Wolf, Jochen
  B. W., 2014. The genomic landscape underlying phenotypic integrity in the face of
  gene flow in crows. Science 344, 1410–1414.
- Remington, D.L., Thornsberry, J.M., Matsuoka, Y., Wilson, L.M., Whitt, S.R., Doebley, J.,
  Kresovich, S., Goodman, M.M., Buckler, E.S., 2001. Structure of linkage
  disequilibrium and phenotypic associations in the maize genome. Proc. Natl. Acad. Sci.
  98, 11479–11484. https://doi.org/10.1073/pnas.201394398
- Runemark, A. *et al.* Variation and constraints in hybrid genome formation. *Nat. Ecol. Evol.*(2018).
- Sankararaman, S., Mallick, S., Dannemann, M., Prüfer, K., Kelso, J., Pääbo, S., Patterson, N.,
  Reich, D., 2014. The genomic landscape of Neanderthal ancestry in present-day
  humans. Nature 507, 354–357. https://doi.org/10.1038/nature12961
- Schiffels, S., Durbin, R., 2014. Inferring human population size and separation history from
   multiple genome sequences. Nat. Genet. 46, 919–925. https://doi.org/10.1038/ng.3015
- Schumer, M., Cui, R., Powell, D.L., Rosenthal, G.G., Andolfatto, P., 2016. Ancient
  hybridization and genomic stabilization in a swordtail fish. Mol. Ecol. 25, 2661–2679.
  https://doi.org/10.1111/mec.13602
- Schumer, M., Rosenthal, G. G. & Andolfatto, P. How common is homoploid hybrid
  speciation?: Perspective. *Evolution* 68, 1553–1560 (2014).
- Sedlazeck, F.J., Rescheneder, P., Smolka, M., Fang, H., Nattestad, M., von Haeseler, A.,
  Schatz, M.C., 2018. Accurate detection of complex structural variations using singlemolecule sequencing. Nat. Methods 15, 461–468. https://doi.org/10.1038/s41592-0180001-7
- Seehausen, O., 2004. Hybridization and adaptive radiation. Trends Ecol. Evol. 19, 198–207.
   https://doi.org/10.1016/j.tree.2004.01.003
- Singh, G., Klar, A.J., 2002. The 2.1-kb inverted repeat DNA sequences flank the mat2, 3
  silent region in two species of Schizosaccharomyces and are involved in epigenetic
  silencing in Schizosaccharomyces pombe. Genetics 162, 591–602.
- Soltis, P.S., Soltis, D.E., 2009. The Role of Hybridization in Plant Speciation. Annu. Rev.
   Plant Biol. 60, 561–588. https://doi.org/10.1146/annurev.arplant.043008.092039
- Speed, D., Hemani, G., Johnson, M.R., Balding, D.J., 2012. Improved Heritability Estimation
   from Genome-wide SNPs. Am. J. Hum. Genet. 91, 1011–1021.
   https://doi.org/10.1016/j.ajhg.2012.10.010
- Stamatakis, A., 2014. RAxML version 8: a tool for phylogenetic analysis and post-analysis of
   large phylogenies. Bioinformatics 30, 1312–1313.
- 907 https://doi.org/10.1093/bioinformatics/btu033

- 908 Steenkamp, E.T., Wingfield, M.J., McTaggart, A.R., Wingfield, B.D., 2018. Fungal species 909 and their boundaries matter – Definitions, mechanisms and practical implications. 910 Fungal Biol. Rev. 32, 104–116. https://doi.org/10.1016/j.fbr.2017.11.002
- 911 Stukenbrock, E.H., 2016. The Role of Hybridization in the Evolution and Emergence of New 912 Fungal Plant Pathogens. Phytopathology 106, 104–112.
- 913 https://doi.org/10.1094/PHYTO-08-15-0184-RVW
- 914 Suzuki, R., Shimodaira, H., 2006. Pvclust: an R package for assessing the uncertainty in 915 hierarchical clustering. Bioinformatics 22, 1540–1542.
- 916 https://doi.org/10.1093/bioinformatics/btl117
- 917 Tajima, F., 1989. Statistical Method for Testing the Neutral Mutation Hypothesis by DNA 918 Polymorphism. Genetics 123, 585–595.
- 919 Taylor, D.J., Hebert, P.D., 1993. Habitat-dependent hybrid parentage and differential 920 introgression between neighboringly sympatric Daphnia species. Proc. Natl. Acad. Sci. 921 90, 7079-7083. https://doi.org/10.1073/pnas.90.15.7079
- 922 Team, R.C., 2014. R: A language and environment for statistical computing.
- 923 Teresa Avelar, A., Perfeito, L., Gordo, I., Godinho Ferreira, M., 2013. Genome architecture is 924 a selectable trait that can be maintained by antagonistic pleiotropy. Nat. Commun. 4, 925 2235. https://doi.org/10.1038/ncomms3235
- The Heliconius Genome Consortium, Dasmahapatra, K.K., Walters, J.R., Briscoe, A.D., 926 927 Davey, J.W., Whibley, A., Nadeau, N.J., Zimin, A.V., Hughes, D.S.T., Ferguson, L.C., Martin, S.H., Salazar, C., Lewis, J.J., Adler, S., Ahn, S.-J., Baker, D.A., Baxter, S.W., 928
- 929 Chamberlain, N.L., Chauhan, R., Counterman, B.A., Dalmay, T., Gilbert, L.E.,
- 930 Gordon, K., Heckel, D.G., Hines, H.M., Hoff, K.J., Holland, P.W.H., Jacquin-Joly, E., 931
- Jiggins, F.M., Jones, R.T., Kapan, D.D., Kersey, P., Lamas, G., Lawson, D., Mapleson, 932 D., Maroja, L.S., Martin, A., Moxon, S., Palmer, W.J., Papa, R., Papanicolaou, A.,
- 933 Pauchet, Y., Ray, D.A., Rosser, N., Salzberg, S.L., Supple, M.A., Surridge, A.,
- 934 Tenger-Trolander, A., Vogel, H., Wilkinson, P.A., Wilson, D., Yorke, J.A., Yuan, F.,
- 935 Balmuth, A.L., Eland, C., Gharbi, K., Thomson, M., Gibbs, R.A., Han, Y., Jayaseelan,
- 936 J.C., Kovar, C., Mathew, T., Muzny, D.M., Ongeri, F., Pu, L.-L., Qu, J., Thornton,
- 937 R.L., Worley, K.C., Wu, Y.-Q., Linares, M., Blaxter, M.L., ffrench-Constant, R.H.,
- 938 Joron, M., Kronforst, M.R., Mullen, S.P., Reed, R.D., Scherer, S.E., Richards, S.,
- 939 Mallet, J., Owen McMillan, W., Jiggins, C.D., 2012. Butterfly genome reveals 940 promiscuous exchange of mimicry adaptations among species. Nature 487, 94–98. 941 https://doi.org/10.1038/nature11041
- 942 Turner, L.M., Harr, B., 2014. Genome-wide mapping in a house mouse hybrid zone reveals 943 hybrid sterility loci and Dobzhansky-Muller interactions. eLife 3, e02504. 944 https://doi.org/10.7554/eLife.02504
- 945 Twyford, A.D., Streisfeld, M.A., Lowry, D.B., Friedman, J., 2015. Genomic studies on the 946 nature of species: adaptation and speciation in Mimulus. Mol. Ecol. 24, 2601–2609. 947 https://doi.org/10.1111/mec.13190
- 948 Vijay, N., Bossu, C.M., Poelstra, J.W., Weissensteiner, M.H., Suh, A., Kryukov, A.P., Wolf, 949 J.B.W., 2016. Evolution of heterogeneous genome differentiation across multiple 950 contact zones in a crow species complex. Nat. Commun. 7, 13195. 951 https://doi.org/10.1038/ncomms13195
- Walker, B.J., Abeel, T., Shea, T., Priest, M., Abouelliel, A., Sakthikumar, S., Cuomo, C.A., 952 953 Zeng, Q., Wortman, J., Young, S.K., Earl, A.M., 2014. Pilon: An Integrated Tool for 954 Comprehensive Microbial Variant Detection and Genome Assembly Improvement. 955
  - PLoS ONE 9, e112963. https://doi.org/10.1371/journal.pone.0112963

- Watterson, G.A., 1975. On the number of segregating sites in genetical models without recombination. Theor. Popul. Biol. 7, 256–276. https://doi.org/10.1016/0040-5809(75)90020-9
- Weir, B.S., 1979. Inferences about Linkage Disequilibrium. Biometrics 35, 235.
   https://doi.org/10.2307/2529947
- Wellenreuther, M., Bernatchez, L., 2018. Eco-Evolutionary Genomics of Chromosomal
   Inversions. Trends Ecol. Evol. 33, 427–440. https://doi.org/10.1016/j.tree.2018.04.002
- Wood, V., Gwilliam, R., Rajandream, M.-A., Lyne, M., Lyne, R., Stewart, A., Sgouros, J., 963 964 Peat, N., Hayles, J., Baker, S., Basham, D., Bowman, S., Brooks, K., Brown, D., 965 Brown, S., Chillingworth, T., Churcher, C., Collins, M., Connor, R., Cronin, A., Davis, 966 P., Feltwell, T., Fraser, A., Gentles, S., Goble, A., Hamlin, N., Harris, D., Hidalgo, J., 967 Hodgson, G., Holrovd, S., Hornsby, T., Howarth, S., Huckle, E.J., Hunt, S., Jagels, K., James, K., Jones, L., Jones, M., Leather, S., McDonald, S., McLean, J., Mooney, P., 968 969 Moule, S., Mungall, K., Murphy, L., Niblett, D., Odell, C., Oliver, K., O'Neil, S., 970 Pearson, D., Quail, M.A., Rabbinowitsch, E., Rutherford, K., Rutter, S., Saunders, D., 971 Seeger, K., Sharp, S., Skelton, J., Simmonds, M., Squares, R., Squares, S., Stevens, K., 972 Taylor, K., Taylor, R.G., Tivey, A., Walsh, S., Warren, T., Whitehead, S., Woodward, 973 J., Volckaert, G., Aert, R., Robben, J., Grymonprez, B., Weltjens, I., Vanstreels, E., 974 Rieger, M., Schäfer, M., Müller-Auer, S., Gabel, C., Fuchs, M., Düsterhöft, A., Fritzc, 975 C., Holzer, E., Moestl, D., Hilbert, H., Borzym, K., Langer, I., Beck, A., Lehrach, H., 976 Reinhardt, R., Pohl, T.M., Eger, P., Zimmermann, W., Wedler, H., Wambutt, R., 977 Purnelle, B., Goffeau, A., Cadieu, E., Dréano, S., Gloux, S., Lelaure, V., Mottier, S., 978 Galibert, F., Aves, S.J., Xiang, Z., Hunt, C., Moore, K., Hurst, S.M., Lucas, M., 979 Rochet, M., Gaillardin, C., Tallada, V.A., Garzon, A., Thode, G., Daga, R.R., Cruzado, 980 L., Jimenez, J., Sánchez, M., del Rey, F., Benito, J., Domínguez, A., Revuelta, J.L., 981 Moreno, S., Armstrong, J., Forsburg, S.L., Cerutti, L., Lowe, T., McCombie, W.R., 982 Paulsen, I., Potashkin, J., Shpakovski, G.V., Ussery, D., Barrell, B.G., Nurse, P., 2003. 983 Erratum: corrigendum: The genome sequence of Schizosaccharomyces pombe. Nature 984 421, 94-94. https://doi.org/10.1038/nature01203
- 985 Wood, V., Gwilliam, R., Rajandream, M.-A., Lyne, M., Lyne, R., Stewart, A., Sgouros, J., 986 Peat, N., Hayles, J., Baker, S., Basham, D., Bowman, S., Brooks, K., Brown, D., 987 Brown, S., Chillingworth, T., Churcher, C., Collins, M., Connor, R., Cronin, A., Davis, 988 P., Feltwell, T., Fraser, A., Gentles, S., Goble, A., Hamlin, N., Harris, D., Hidalgo, J., 989 Hodgson, G., Holroyd, S., Hornsby, T., Howarth, S., Huckle, E.J., Hunt, S., Jagels, K., 990 James, K., Jones, L., Jones, M., Leather, S., McDonald, S., McLean, J., Mooney, P., 991 Moule, S., Mungall, K., Murphy, L., Niblett, D., Odell, C., Oliver, K., O'Neil, S., 992 Pearson, D., Quail, M.A., Rabbinowitsch, E., Rutherford, K., Rutter, S., Saunders, D., 993 Seeger, K., Sharp, S., Skelton, J., Simmonds, M., Squares, R., Squares, S., Stevens, K., 994 Taylor, K., Taylor, R.G., Tivey, A., Walsh, S., Warren, T., Whitehead, S., Woodward, 995 J., Volckaert, G., Aert, R., Robben, J., Grymonprez, B., Weltjens, I., Vanstreels, E., 996 Rieger, M., Schäfer, M., Müller-Auer, S., Gabel, C., Fuchs, M., Fritzc, C., Holzer, E., 997 Moestl, D., Hilbert, H., Borzym, K., Langer, I., Beck, A., Lehrach, H., Reinhardt, R., 998 Pohl, T.M., Eger, P., Zimmermann, W., Wedler, H., Wambutt, R., Purnelle, B., 999 Goffeau, A., Cadieu, E., Dréano, S., Gloux, S., Lelaure, V., Mottier, S., Galibert, F., 1000 Aves, S.J., Xiang, Z., Hunt, C., Moore, K., Hurst, S.M., Lucas, M., Rochet, M., 1001 Gaillardin, C., Tallada, V.A., Garzon, A., Thode, G., Daga, R.R., Cruzado, L., 1002 Jimenez, J., Sánchez, M., del Rey, F., Benito, J., Domínguez, A., Revuelta, J.L., 1003 Moreno, S., Armstrong, J., Forsburg, S.L., Cerrutti, L., Lowe, T., McCombie, W.R., Paulsen, I., Potashkin, J., Shpakovski, G.V., Ussery, D., Barrell, B.G., Nurse, P., 2002. 1004

1005	Erratum: The genome sequence of Schizosaccharomyces pombe. Nature 415, 871–880.
1006	https://doi.org/10.1038/nature724
1007	Zanders, S.E., Eickbush, M.T., Yu, J.S., Kang, JW., Fowler, K.R., Smith, G.R., Malik, H.S.,
1008	2014. Genome rearrangements and pervasive meiotic drive cause hybrid infertility in
1009	fission yeast. eLife 3, e02630. https://doi.org/10.7554/eLife.02630
1010	Zheng, X., Gogarten, S.M., Lawrence, M., Stilp, A., Conomos, M.P., Weir, B.S., Laurie, C.,
1011	Levine, D., 2017. SeqArray—a storage-efficient high-performance data format for
1012	WGS variant calls. Bioinformatics 33, 2251–2257.
1013	https://doi.org/10.1093/bioinformatics/btx145
1014	Zheng, X., Levine, D., Shen, J., Gogarten, S.M., Laurie, C., Weir, B.S., 2012. A high-
1015	performance computing toolset for relatedness and principal component analysis of
1016	SNP data. Bioinformatics 28, 3326–3328.
1017	https://doi.org/10.1093/bioinformatics/bts606
1018	
1019	
1020	
1021	Figure legends
1022	

1023 Figure 1 | Distribution of Sp (red) and Sk (blue) ancestry blocks along the S. pombe 1024 genome. (a) Example of principal component analysis (PCA) of a representative genomic 1025 window in chromosome I (top) and the whole mitochondrial DNA (bottom). Samples fall into 1026 two major clades, Sp (red square) and Sk (blue square). The proportion of variance explained 1027 by PC1 and PC2 is indicated on the axis labels. Additional examples are found in 1028 Supplementary Figure 1 (b) Proportion of variance explained by PC1 (black line) and PC2 (grey line) for each genomic window along the genome. Centromeres are indicated with red 1029 1030 bars. Note the drop in proximity to centromeres and telomeres where genotype quality is significantly reduced. (c) Heatmap for one representative of 57 near-clonal groups indicating 1031 ancestry along the genome (right panel). Samples are organised according to a hierarchical 1032 1033 clustering, grouping samples based on ancestral block distribution (left dendrogram). Colours 1034 on the tips of the cladogram represent cluster membership by chromosome (see 1035 Supplementary Figure 7). Samples changing clustering group between chromosomes are shown in grey. (d) Estimate of  $D_{xy}$  between ancestral groups and genetic diversity ( $\pi$ ) within 1036 1037 the Sp (red) and Sk clade (blue) along the genome.

**Figure 2** | **Population genetic summary statistics.** (a) Proportion of Sp (red) and Sk (blue) ancestry across all 57 samples along the genome. (b) Tajima's D differentiated by Sp (red) and Sk (blue) ancestry and pooled across all samples irrespective of ancestry (grey line). Genomic regions previously identified under purifying selection (Fawcett et al., 2014) are shown with black triangles. Reported active meiotic drives (Zanders et al., 2014; Hu et al., 2017; Nuckolls et al., 2017) are indicated by yellow triangles. The third panel shows the difference between ancestry specific Tajima's D and the estimate from the pooled samples.

1046

Figure 3 | Inferred evolutionary history of contemporary *S. pombe* strains. An ancestral population diverged into two major clades, *Sp* (red) and *Sk* (blue) since approximately 2300 years ago (Jeffares et al., 2015). Recurrent hybridization upon secondary contact initiated around 20 sexual outcrossing generations ago resulted in admixed genomes with a range of admixture proportions (bottom) prevailing today.

1052

1053 Figure 4 | Ancestry explains variation in phenotype and reproductive isolation. (a) PCA 1054 of normalized phenotypic variation across 228 traits. The proportion of variance explained by 1055 PC1 and PC2 is indicated on the axis labels. Admixed samples (dots) are coloured coded by 1056 ancestry proportion (cf. Figure 3) ranging from pure Sp (red triangle) to pure Sk (blue 1057 triangle) ancestry. (b) Phenotypic distribution of example traits separated by the degree of 1058 admixture: admixed samples are shown in grey, pure ancestral Sp and Sk samples are shown 1059 in red and blue respectively. The number of traits corresponding to a dominant, additive and 1060 transgressive genetic architecture is indicated on the right hand side (c) Comparison of 1061 heritability estimates of all 228 traits based on 172,935 SNPs (abscissa) and on 1925 genomic 1062 windows polarized by ancestry (ordinate). Colours indicate statistical significance. NS: 1063 heritability values not significantly different from zero, AncHap: significant only using

ancestral blocks, *SNPs:* significant only using SNPs, *SB:* significant in both analyses.
Diagonal (slope=1) added as reference. (d) Histogram of the difference between heritability
estimates using SNPs and ancestry components for all 228 traits. (e) Correlation between the
difference in ancestry proportions between two strains (cf. Figure 2) and spore viability of the
cross. Red box shows samples with low spore viability but high genetic similarity.

1069

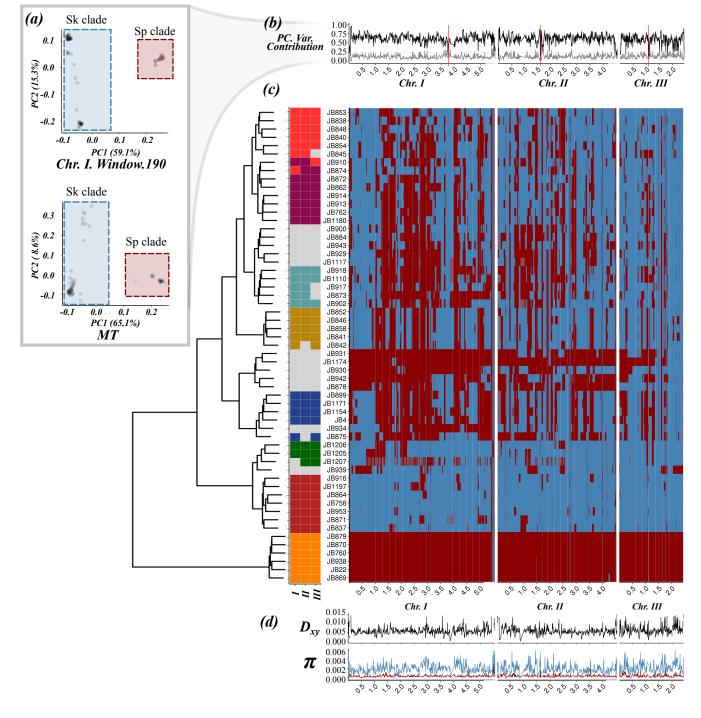
Figure 5 | Characterization of structural variation based on long-read, real-time 1070 1071 sequencing. (a) Schematic representation of the three chromosomes in different strains 1072 displaying SVs larger than 10kb relative to reference genome JB22 (left panel). Chromosome 1073 arms are differentiated by colour; orientation is indicated with arrows relative to the reference; 1074 black bars represent centromeres. In the second panel, additional SVs, their type and ID of the corresponding strain are illustrated in brackets. (b) Size distribution of SVs below 10 kb. 1075 1076 Colours indicate the type of SV. (c) Distribution of SV density along the genome. Black bars 1077 represent centromeres. (d) Two-dimensional, folded site frequency spectrum between inferred 1078 ancestral populations for all SVs, SNPs and LTR INDELs. Numbers and colours show the 1079 percentage of the total number of variants in each category. Variants with low frequency in both populations are shown in the blue box. Variants highly differentiated between 1080 populations are show in red boxes with total in the upper right box. Fills with percentage 1081 1082 lower than 0.01 are empty.

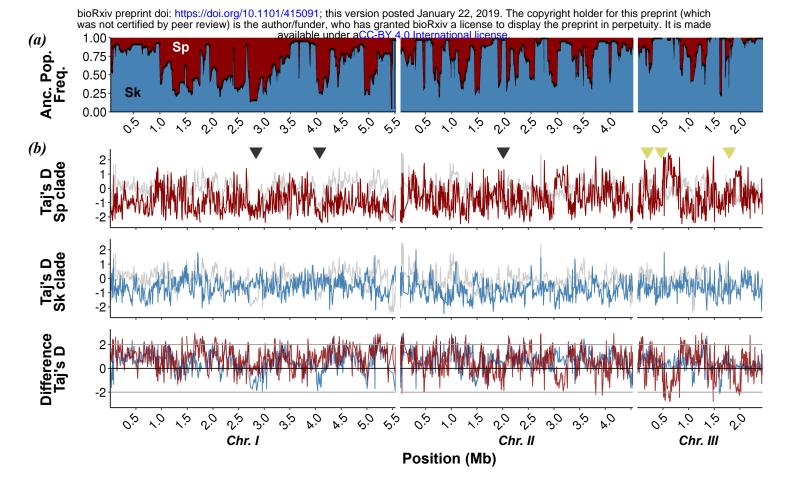
1083 Abbreviations: DEL: deletion; DUP: duplication; INS: insertion; INV: inversion

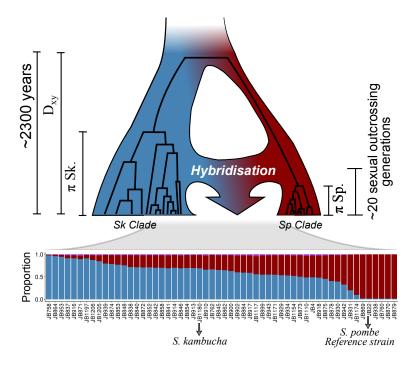
1084

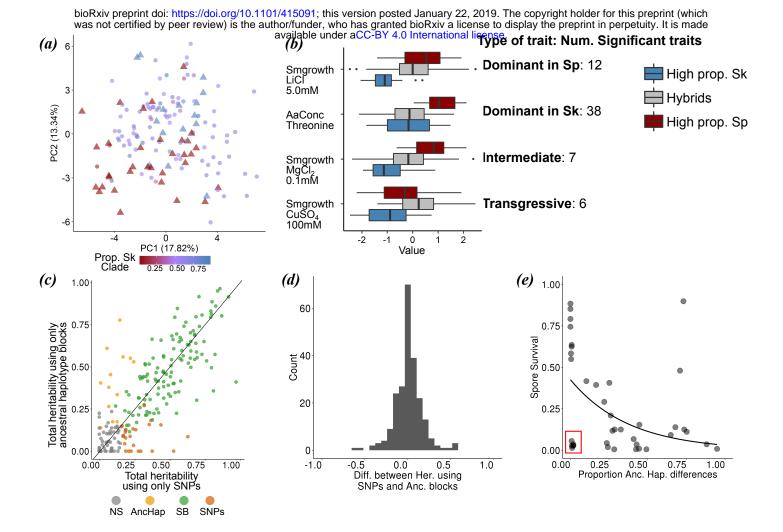
Figure 6 | Decay in linkage disequilibrium (LD) with genetic distance. Relationship
between LD (R<sup>2</sup>) and physical distance is depicted for each chromosome. Black points
represent values for each window pair comparison. Lines show non-lineal regression model
based on Hill & Weir (1988) and Remington et al. (2001). LD estimates were divided into

- 1089 three categories representing comparison between windows of shared ancestry (Sp-Sp or Sk-
- 1090 *Sk*) reflecting positive ancestry disequilibrium (AD) or of opposite ancestry (*Sk-Sp*) reflecting
- 1091 negative AD.









bioRxiv preprint doi: https://doi.org/10.1101/415091; this version posted January 22, 2019. The copyright holder for this preprint (which was not certified by peer review) is the author/funder, who has granted bioRxiv a license to display the preprint in perpetuity. It is made available under a CC-BY 4.0 International license.

